Fabrication and characterization two step stir casting with ultrasonic assisted novel AA7150-hBN nanocomposites

Pagidi Madhukar [a, *], N. Selvaraj [a], C.S.P. Rao [b], G.B. Veeresh Kumar [c]

[a] Department of Mechanical Engineering, National Institute of Technology, Warangal, Telangana State, 506004, India
[b] National Institute of Technology-Andhra Pradesh, Tadepalligudem, Andhra Pradesh, 534102, India
[c] Department of Mechanical Engineering, National Institute of Technology-Andhra Pradesh, Tadepalligudem, Andhra Pradesh, 534102, India

ARTICLE INFO

ABSTRACT

The Al7150 alloy plays a vital role in aerospace and automotive industry applications due to its extraordinary characteristics like strength to weight ratio, toughness and fatigue resistance. But in the current scenario researchers are looking for significant improvement in wear resistance at various service loads. It is in such a context this paper deals with the fabrication, mechanical and wear resistance properties investigation of the Al7150-hBN nanocomposites, which is fabricated through ultrasonic assisted double Stir casting technique and compared with monolithic material. The microstructure studies were carried out through Optical Microscope (OM) for grain structure, Scanning Electron Microscope (SEM) for particle distribution, ultimate tensile strength including the morphological studies related to fracture surface and Energy Dispersive X-ray (EDX) spectroscopy for elemental analysis. The pin on disc tribometer was used to study the tribological characteristics of the developed nano-composite materials by varying the applied loads and weight percentage of hBN reinforcement at a constant sliding speed and distance. The SEM images of the worn-out surfaces were studied extensively to study the tribological properties.

© 2019 Elsevier B.V. All rights reserved.

1. Introduction

Aluminum (Al) based alloys are highly attractive materials to aerospace and atomic structure applications due to their light-weight properties but they suffer from poor wear resistance. For improving the desired properties of these alloys, Al Metal Matrix Composites (MMCs) were introduced by adding reinforcement particles. These reinforcements act as second phase particles to improve the properties of Al-MMCs and ensure environmental benefits. Therefore, Al-MMCs are widely using in structural applications instead of monolithic and other engineering materials like ferrous and nonferrous alloys. Al-MMCs are playing a major role in aerospace and automotive applications [1] due to their strength to weight ratio and low density. From the last two decades [2], several manufacturing methods are available to produce Metal Matrix Composites (MMCs) which can be classified into two major types. One is solid state fabrication process and another one is liquid state fabrication process. In solid state, mechanical milling and

mechanical alloying [3] are used to improve the mechanical properties of MMCs. This enhancement mainly due to re-welding of fractured particle, cold welding and flattering of particles during ball milling. For decreasing porosity and homogeneous distribution of particles, secondary processes are used like extrusion and forging or rolling methods. In case of liquid state, processes classified like stir casting [4], compocasting [5], squeeze casting [6], in-situ synthesis [7] and liquid metal infiltration [8–10]. From the above methods, stir casting is more economical and prominent method to fabricate bulk quantity of MMCs [11]. The reinforcement particles are sorted out into two different sizes: micro and nano. The micro reinforcements enhance engineering properties but lower the ductility. In recent years, nano-sized reinforcements have been introduced and used in place of micro-particles due to its high surface to volume ratio (1000 times more) compared to the micro-particles area [12], which results in superior performance. Few researchers have proved that the alloy has enhanced fatigue life as well as high resistance to temperature creep [5,13], however, the preparation of Al-MMCs with the nano-sized particles in liquid pool is very difficult to distribute homogeneously because of its poor wettability, clusters and agglomerations formation. In such

Table 1
Chemical composition of Al7150 in weight percentages (wt%).

Chemical Composition	Mg	Zn	Cu	Fe	Zr	Si	Mn	Al
AA7150	2.56	6.37	2.25	0.12	0.11	0.08	0.009	Balance

attempts, the ultrasonic assisted stir casting provides a good platform for homogeneous distribution of nanoparticles in Al alloy melt [14–17]. The liquid metallurgy route is a highly recommended technique to manufacture the Al-MMCs, because of the flexibility and low cost [4]. For example, Qiang Li et al. [18], used ultrasonic vibration assisted stir casting to disperse the nanoparticles and studied the solidification behavior, engineering and microstructural properties. Wei-Si-Tian et al. [19], fabricated micro and nano-sized Titanium Carbon particulate (TiC_p) composites through in-situ process and studied ductility and strength at room temperature as well as elevated temperatures. S Mahathanabodee et al. [20], presented SS316L/hBN composites through P/M technique and studied the effect of hexagonal Boron Nitride (hBN) on mechanical as well as tribological properties. Gisele Hammes et al. [21], prepared Fe–Si–C based matrix composites through P/M route and studied the effect of hBN and Graphite (Gr) solid lubricants effect on MMCs and examined the mechanical and wear characteristics, which contain 1%hBN and 9% Gr. Niloofar et al. [3], produced a new generation 10Ce-TZP/Al_2O_3 composites through P/M method. Aqueous combustion technique is performed particle reinforced Aluminium Matric Composites (AMCs). Erosion, mechanical and wear properties were investigated and found to be enhanced by incorporation of reinforcement particles.

A novel technique was used in this paper by combining the ultrasonic vibration, double stir casting and vertex method to fabricate AA7150-hBN nanocomposites to obtain uniform distribution of nanoparticles into the molten metal. Microstructure analysis through optical and scanning electron microscopy was investigated for crystal refinement and particle distribution. Dry sliding wear test was performed on pin-on-disk tribometer and their worn surfaces were investigated for wear characterization. The main aim of current work is to find the influence of hBN nanoparticle reinforcement and ultrasonic effect on the characteristics of AA7150-hBN nanocomposites.

2. Materials and methods

In the present study, Al7150 alloy was selected as the matrix and purchased from Venuka Engineering Private Limited, Hyderabad, India. The chemical composition of Al7150 is shown in Table 1. Hexagonal Boron Nitride (h-BN) nano-powder was selected as reinforcement and purchased from Sisco Research laboratories private limited, India. The amount of hBN nano reinforcement was varied from 0 wt% to 3 wt% in the steps of 0.5 wt%. The average particle size of h-BN is 70 nm. Hexachloroethane (C_2Cl_6) and Magnesium (Mg) purchased from Taranath Scientific & Chemical Company, Hanamkonda. Mechanical stirrer was coated with ZrO_2 (melting point: 2,715 °C) to improve the temperature resistance of stirrer blade. Table 2 is presented with mechnaical properties of

AA7150 matrix and hBN partculates.

AA7150 was charged into the graphite crucible and heated up to 750 °C. The temperature was maintained between 750 °C to 800 °C for an hour to complete the melting of AA7150 and C_2Cl_6 degassing tablet was used to minimize the gasses in aluminium melt. Coarser grain size Mg particles were used as flux to improving the wettability of reinforcements during the stirring of molten liquid. Double stir casting technique was adapted and used to disperse the nanoparticles into the liquid. Pre-heated hexagonal boron nitride (h-BN at 450 °C for 30 min to make the compatibility with liquid metal, avoid of organic impurities as well as moisture) was added into the liquid metal pool and stirred with a mechanical stirrer at vertex formation speed (350–400 rpm). It continued for 20 min, in terms of two equal step size. Each step was 10 min of stirring action followed by the formation of semisolid state between the steps. Due to the addition of nanoparticles, the viscosity of aluminium alloy melt automatically improved. To reduce the viscosity, flowability of nanoparticles in a liquid material was increased, and to ensure the efficiency of the sonication process, higher melting temperature was maintained at 800 °C inside the crucible. Then the ultrasonic cavitation process was done with titanium alloy probe (high-temperature resistance) for 10 min by dipping ¾ of ultrasonic probe into molten liquid. After the sonication process, the mechanical stirrer was used for 5 min to stir the liquid metal to disperse the blasted clusters and agglomerations of reinforcement nanoparticles. Then molten liquid was poured immediately into a pre-heated (500 °C) die-steel mould as well as allowed to cool by natural cooling cycle at atmospheric temperature for the next 24 h. The solidified cylindrical work pieces were removed from the mould and the specimens were machined as per ASTM standards for various testing.

The Al7150-hBN nanocomposite microstructure analysis was performed by SEM Tescon Make: Vega 3 LMU Model and elemental analysis was carried out with the help of EDS Oxford Instruments, U.K to capture SEM images. The Al7150 alloy and its nanocomposite samples were polished with the help of different grades of emery papers along with disc polishing. Keller agent was used for 23–25sec to get the microstructure. X-Ray Diffraction Model: Panalytical X'pert Powder was used to examine the Al7150-hBN nanocomposites and to study and confirm the presence of base metal as well as reinforced particulates in elemental analysis.

The density of monolithic and various weight percentage reinforced composites were calculated using Archimedes principle, which involves weight in air as well as weight in water. Porosity plays a critical role to decide the properties of material in the casting process. The porosity levels are normal but, while incorporating the particles, the atmosphere air interact with particles, resulting in porosity. Avoiding porosity is very difficult but it can be minimizing and controlled during the process. Hardness of the Al7150 alloy and hBN particulates reinforced nanocomposites were evaluated using Vicker's micro-hardness tester using Economet VH 1MD equipment with 2 kgf, as per ASTM standard. The experiment was performed on test surface by applying 200 g load for 15sec dwell time. The Ultimate Tensile Strength (UTS) tests were conducted on Al7150 alloy and hBN particulates reinforced nanocomposite samples (T6 condition) using Universal Testing Machine

Table 2
Mechanical properties of AA7150 and hBN particles.

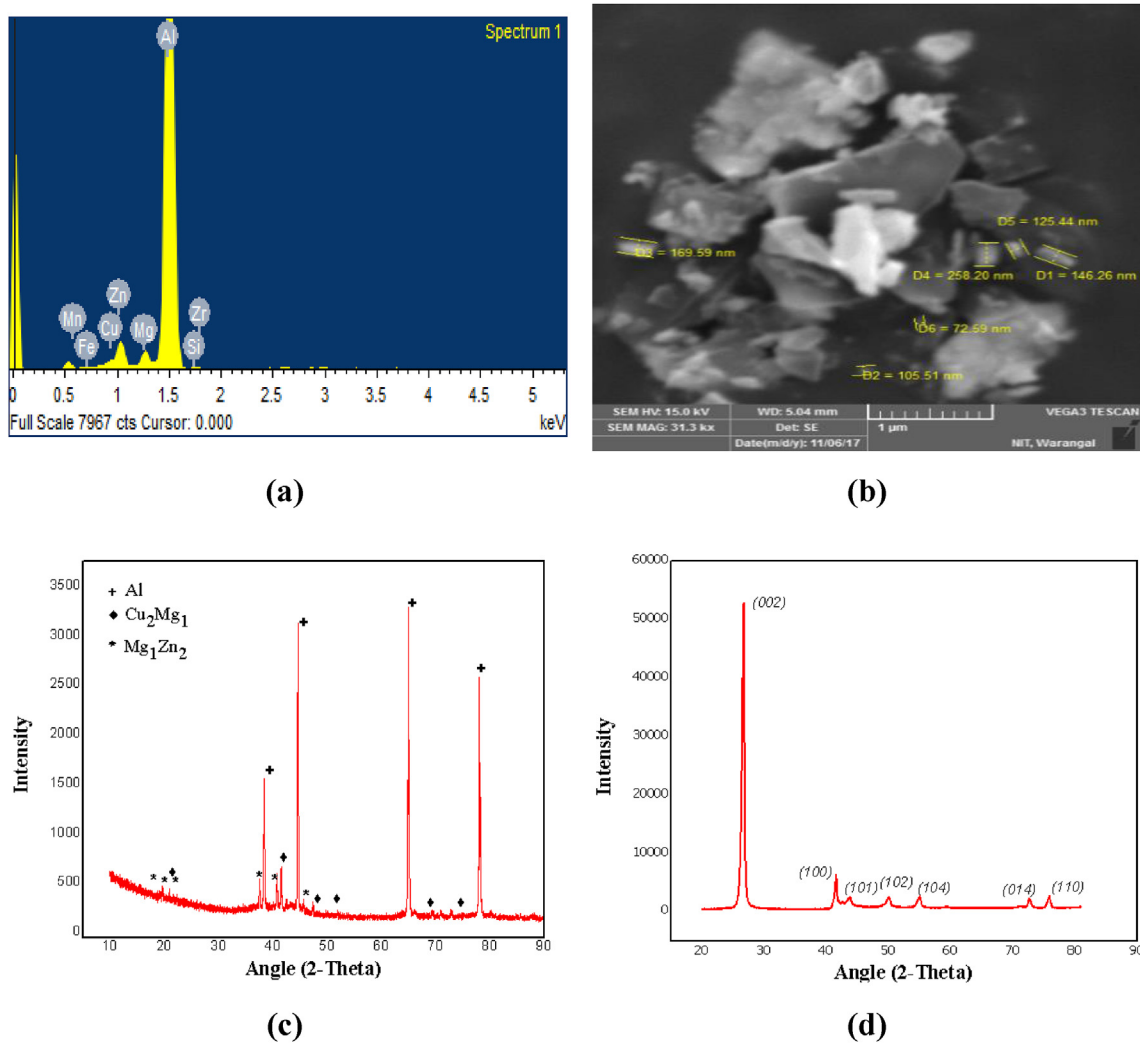| Material	Elastic Modulus (GPa)	Density (g/cc)	Hardness Vickers	Tensile Strength (MPa)
AA7150	71	2.83	140	160
hBN	64.8	2.21	19–192	2.41

(a)

(b)

(c)

(d)

Fig. 1. (a) EDS spectrum of the Al7150 (b) SEM image of hBN nanoparticles (c) XRD Pattern of Al7150 (d) XRD Pattern of hBN nanoparticles.

Table 3
Experimental, Theoretical densities and Porosity of nanocomposites.

%Wt	Ex-Density	Th-Density	Porosity	% Porosity
AA7150	2.7718	2.8300	0.0206	2.0565
0.50%	2.8024	2.8250	0.0080	0.8000
1.00%	2.8082	2.8200	0.0042	0.4184
1.50%	2.8100	2.8150	0.0018	0.1776
2.00%	2.7854	2.8100	0.0088	0.8754
3.00%	2.7700	2.8000	0.0107	1.0714

Fig. 2. Experimental density, percentage of porosity vs different wt.%.

(UTM) of Make: *Blue Star* WDW-100 S with a cross-head speed of 0.5 mm/min at atmospheric temperature and the fracture surfaces were captured with SEM. The tribological experiments were carried out at room temperature on Pin-on-Disc tribometer by varying the different input parameters such as wt% of hBN (0.5−2.0%), applied load (10−40 N) against EN 31 stainless steel having 60HRC hardness. The output responses such as Coefficient of Friction (COF), Wear loss and Temperature (^{o}C) were taken noted from the Linear Variable Differential Transformer (LVDT).
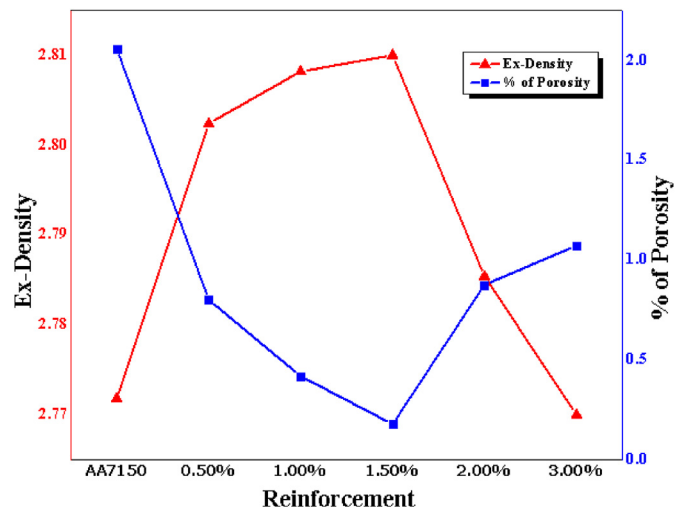
Table 4
Hardness values of monolithic and nanocomposites.

Reinforcement	Hardness (HV)
AA7150	151.3
0.50%	177.6
1.00%	179.4
1.50%	180.2
2.00%	176.4
3.00%	160.8
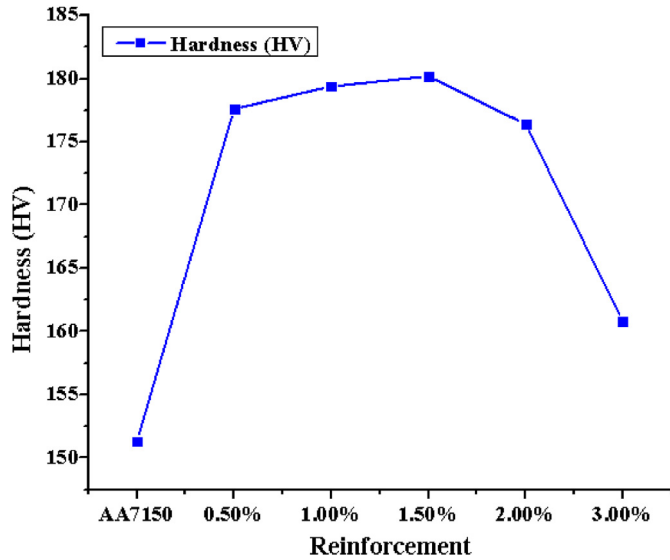
Fig. 3. Hardness vs different wt.%hBN.

Fig. 4. Stress vs Strain curve of monolithic and reinforced nanocomposites.
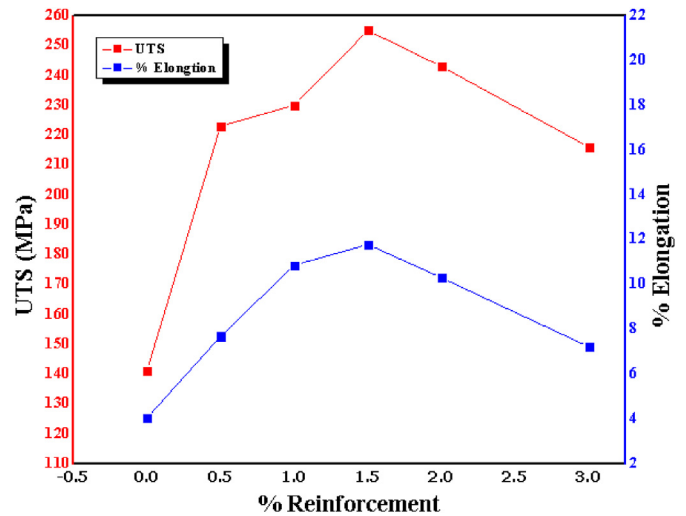
Fig. 5. Ultimate strength, %Elongation vs weight percentage.

3. Results and discussions

Fig. 1 a-b shows the EDS report and SEM photograph of hBN nanoparticles. EDS spectrum, the peaks are indicating with the major elements in monolithic such as Al, Mg, Zn, Cu. The hBN image indicates the size of the particle. The intensity peaks from XRD confirms the Al, Cu_2Mg_1, Mg_1Zn and special number for hBN. The X-Ray diffraction of Al7150 and hBN nanoparticles are shown Fig. 1 c-d.

3.1. Material properties

The results are represented in Table 3 and the respective graphs for both experimental density and porosity are shows in Fig. 2. The theoretical density is decreasing with increasing hBN reinforcement particles due to its low density. The experimental density by Archimedes Principle and theoretical density was calculated using rule of mixture. In the present study, it was noticed that the density is increasi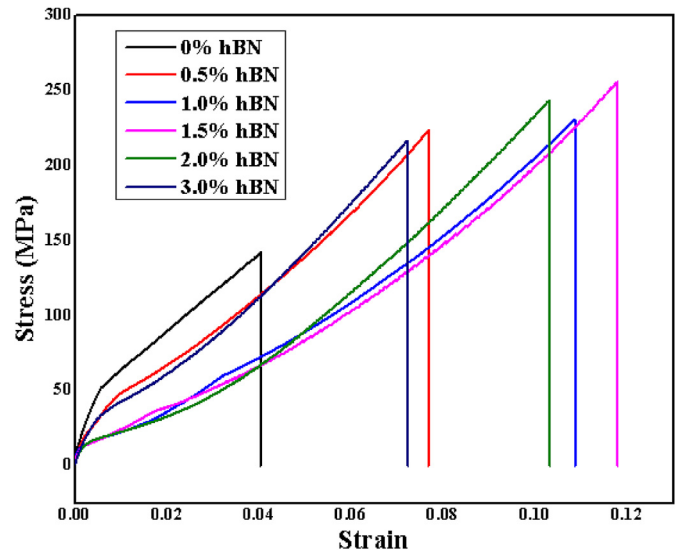ng due to ultrasonic degassing effect which minimizes the porosity and % of porosity decreases due to ultrasonic cavitation effect in the present work [22,23] as well as closely packed uniform distribution of nanoparticles due to ultrasonic streaming effect [24]. Further addition of reinforcement particles decreases the density due to agglomerations that create voids [25].

The resistance offered by the material for indentation was experimentally measured as per ASTM G92. The results of hardness test using Vicker's hardness tester were evaluated and represented in Table 4 and the graphical trend is shown in Fig. 3. From graph, it

Table 5
Mechanical properties and Average grain size of each composition.

S. No.	Sample	Hardness HV	UTS MPa	% Elongation	Avg Grain Size μm
1	AA7150	151.3	141	4.03	76
2	AA7150 + 0.5%hBN	177.6	223	7.684	53
3	AA7150 + 1.0%hBN	179.4	230	10.86	33
4	AA7150 + 1.5%hBN	180.2	255	11.78	17
5	AA7150 + 2.0%hBN	176.4	243	10.30	26
6	AA7150 + 3.0%hBN	160.8	216	7.22	34

%Wt	Optical Microscope	SEM
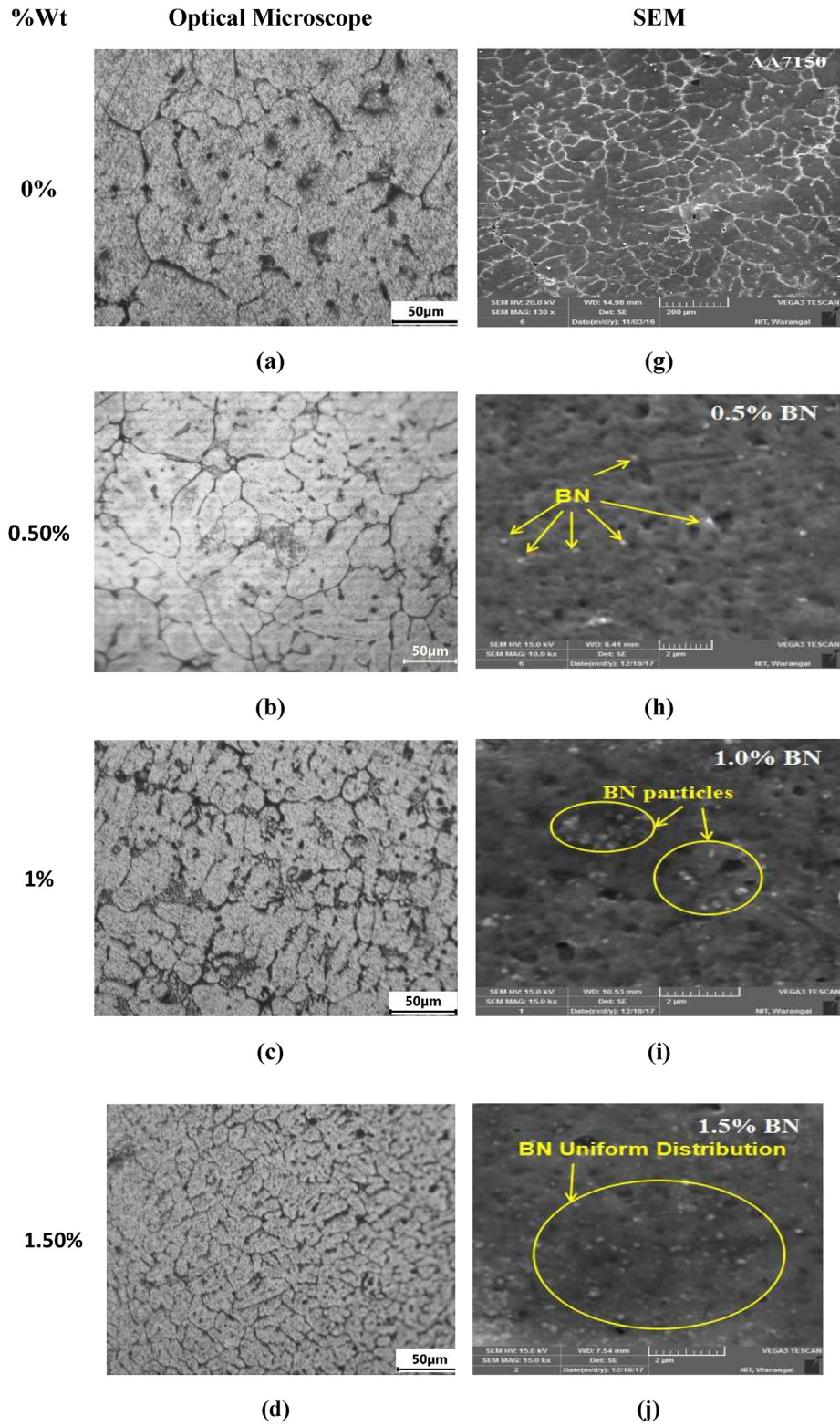
Fig. 6. (a)–(f) Optical Microstructure images and (g)–(l) SEM images of AA7150, 0.5%, 1.0%, 1.5%, 2.0%, 3.0% hBN reinforcement particles.
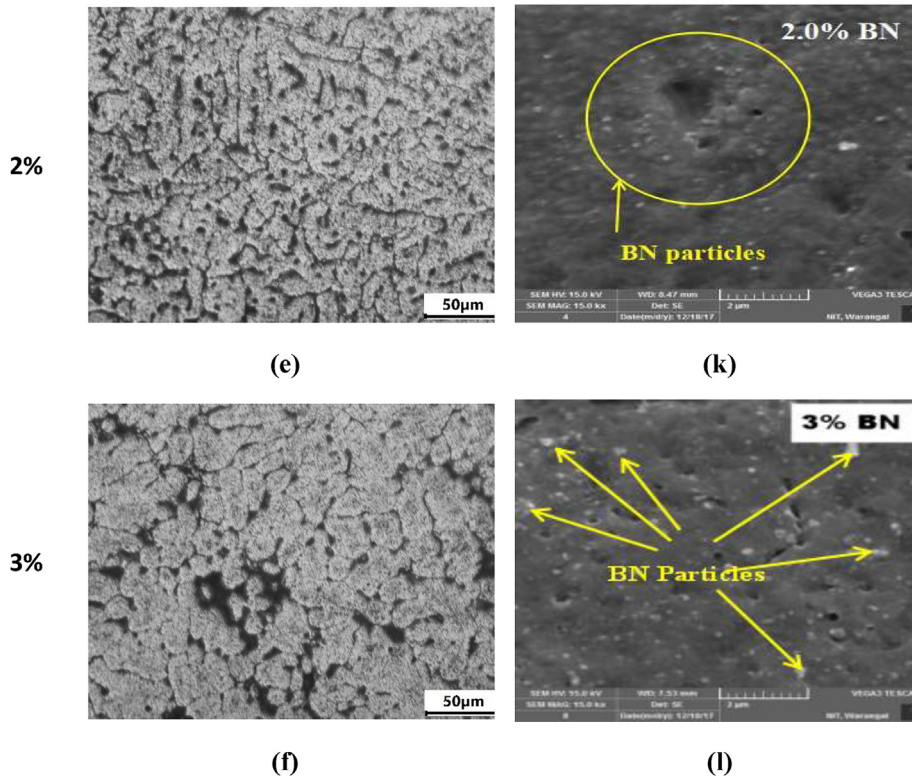
(e)   **(k)**

(f)   **(l)**

Fig. 6. (*continued*).

was noticed that the microhardness of hBN nanoparticle reinforced composite significantly enhanced and 1.5 wt%hBN reinforcement has showed highest hardness of Al7150-hBN nanocomposite material due to hard ceramic particles and decreased internal distance between particles which resist the dislocation movement [26]. The amount of enhancement in microhardness was noticed from 0 to 1.5 wt% hBN is 19.10% and further weight percentages, microhardness decreases due to agglomerations/clusters formation during the mixing [27,28]. The enhancement in microhardness of hBN reinforced nanocomposite is mainly because of grain refinement, good bonding between matrix and ceramic nanoparticles reinforcement, hBN hard phase particles and tight adhesion between hBN as well as matrix material [29,30].

The UTS for Al7150 and its hBN nano-particulates reinforced composites are discussed under this section. The UTS experiments were conducted in accordance with ASTM E8M standards. Table 5 shows the results of hardness, UTS, %'elongation and Average Grain Size (AGS) of monolithic and nanocomposites as well. The fracture surface of tensile strength test specimens was studied through SEM pictograph. Fig. 4 shows the results of tensile test of monolithic and reinforced nanocomposites of hBN particles at atmospheric temperature. The observations were made based on the results that the ultimate strength increases with increasing weight percentage of hBN content up to 1.5 wt% due to higher dislocation between nanoparticles as well as base material along with the larger surface area of hard hBN phase particles [31–34]. Enhancement of properties rightly attribute to the grain refinement, higher load transformation capacity, uniform distribution of particles and large interfacial area [26]. Moreover, the following assumptions could be contemplate: (i) Thermal mismatch, (ii) Dislocation

density, (iii) Orowan strengthening [35,36]. Further improvement in hBN content leads the strength diminishing due to voids, clusters and agglomerations, which advance the failure [37]. The percentage of elongation also follows the same trend for up to 1.5 wt% hBN and then decreases and is shown in Fig. 5.

3.2. Microstructure analysis

Fig. 6a–f, show the optical microscope images of monolithic and nanocomposites. In the optical microscope; the images showed that the elements are segregated at the boundaries for matrix materials and the size of the grains reduces (grain refinement) with the content of hBN reinforcement [38,39] resulting in improvement in mechanical properties [40].

SEM images in Fig. 6g–i shows the alloying elements distribution in the unreinforced Al7150 alloy and Al7150-hBN reinforced nanocomposites and with reference to all the images, the SEM image of the nanocomposite containing 1.5 wt% hBN, Fig. 6 j shows uniform distribution with fewer voids and better grain refinement as compared to 2% & 3% of hBN, which leads to better mechanical properties [41]. With respect to the above discussion it is conclude that Fig. 6 j 1.5 wt% hBN shows uniform distribution. According to Hall-Pitch effect, the grain refinement and fine grains show better properties for uniformly distributed particles.

There are several techniques to support the strengthening of MMCs. Each technique is individual and does not depend on a unique technique but may act simultaneously. The current article used grain refinement and fracture surface analysis to predict the strength [42]. From Fig. 6 (a)–(f), it is observed that there is grain refinement at each composition. The AGS can be measured by using

Linear Intercept Method and Planimetric (Jeffries) Method [43]. In this article, Linear Intercept Method was used to find the average grain size on principle planes (Transfer and Longitudinal directions) of each microphotograph with the help of ImageJ software. The measured values are determined by a formula ($AGS = \frac{\text{Length of the line}}{\text{Number of grains}}$) to get the size of grain. The calculated results for monolithic and nanocomposites are presented in Table 5. From the results, the finer grain size was confirmed in 1.5 wt% hBN nanocomposite matrix when compared to its counter parts. Hence, it is understood that 1.5 wt% hBN shows superior mechanical properties for Al7150-hBN nanocomposites [26].

SEM images of tensile fracture surface at 200 μm scale for monolithic, 1.5 wt% hBN and 3.0 wt% hBN reinforced nano-composites are shown in Fig. 7 and also enlarged images for easy analysis was presented. Fig. 7 a represents many voids, cracks and grape-liked dendrites and the enlarged picture attributes of the grain are caused due to grain detachment; these are confirmed as brittle fracture in nature. Fig. 7 b represents the image at 1.5 wt% hBN reinforced nanocomposite, which results in superior properties, with fewer voids, cracks, facets and grape-like dendrites. The enlarged scale image shows the facets, step-wise dendrites and its

attribute in B−N strength between adjacent layers of crystal structure, which elevate the surface energy as well as the interface friction required for particles to detach. Hence, it confirms the semi brittle in nature [44−46]. 3.0 wt% hBN reinforced SEM image comes with larger voids and cracks as compared with other two composites considered in the present study, which confirmed the decline in properties beyond 1.5%wt hBN nano-particulate reinforced composites.

3.3. Wear behaviour

The tribological studies related to the fabricated materials were conducted on a fully computerized tribometer at room temperature under dry sliding conditions, the wear experiments at a load of 10−40 N while the sliding distance 3000 m was maintained and sliding speed of 2 m/s was considered and maintained constant. ASTM G-99 standard was followed for the conduction of the tribo experiments with cylindrical specimens of dimensions 8 mm in diameter and 30 mm in length used for the experiments. The weight loss of the samples was measured with electronic weighing balance for different loads, wt% of hBN and other output responses with LVDT. The average surface roughness of the Al7150 alloy and its composites pin and disc were maintained to 0.1 μm Ra.

Fig. 8 a-d shows the wear loss of sliding distance 3000 m at a load of 10−40 N and it was observed that the wear loss of the monolithic and nanocomposites increases with increasing of sliding distance due to friction between the sliding surfaces hence the higher temperature rise [47] at larger distances leads to soften the pin material and heavy deformation at contact point results in more wear loss. The wear loss of the hBN reinforced nano-composites was significantly reduced as compared to monolithic material up to 1.5 wt% hBN due to the hardness enhancement, results in seizure and wear resistance improvement of materials. Further higher percentages of hBN leads to reduce the wear resistance due to lower the hardness and the same has been shown in Fig. 8 h. Fig. 8 e-g shows the influence of applied load on wear and temperature rise. The graphical trend was confirmed that the load has greatest significant effect and the most influencing tribological parameter. As the load increases, increases the wear loss and temperature due to higher frictional forces. Fig. 8 h also shows the wear loss against to wt% at 25min time period also attribute that the load increase on the nanocomposites, improves the wear loss respectively. Fig. 8 i shows that the load increases, increases the wear and temperature rise [48,49]. When the load is low, oxides form on the surfaces of the composites and intact with the metal contact surfaces. These oxides significantly affect the tribo characteristics, results in lower COF and wear rate. Further, when the applied load increased, the heat at contact surface is also increased and worn out the oxide layers, therefore the oxide layers are no longer capable of preventing layers at metallic contact surfaces, this frictional heat softens the pin material, resulting in enhancement in the grain size. This is attributed to more contact surface area and increase in wear loss, and further change in delamination with further increase of load [50−53]. The Coefficient of Friction at maximum load at 40 N load, Fig. 8 j shows that COF decreases with increasing hBN wt% content as compared to monolithic material due to the interaction of lubricating film with self-mated couples and this leads to smooth contact surface while reducing the COF [54−56].

Fig. 9a−b SEM images display the monolithic worn surface at minimum load 10 N and maximum load 40 N. 10 N image disclose patches of seriously damaged domains, as well as deep abrasion grooves due to lower load [33] and it leads to severe wear. Fig. 9 b shows the worn surface of the monolithic alloy at a maximum load
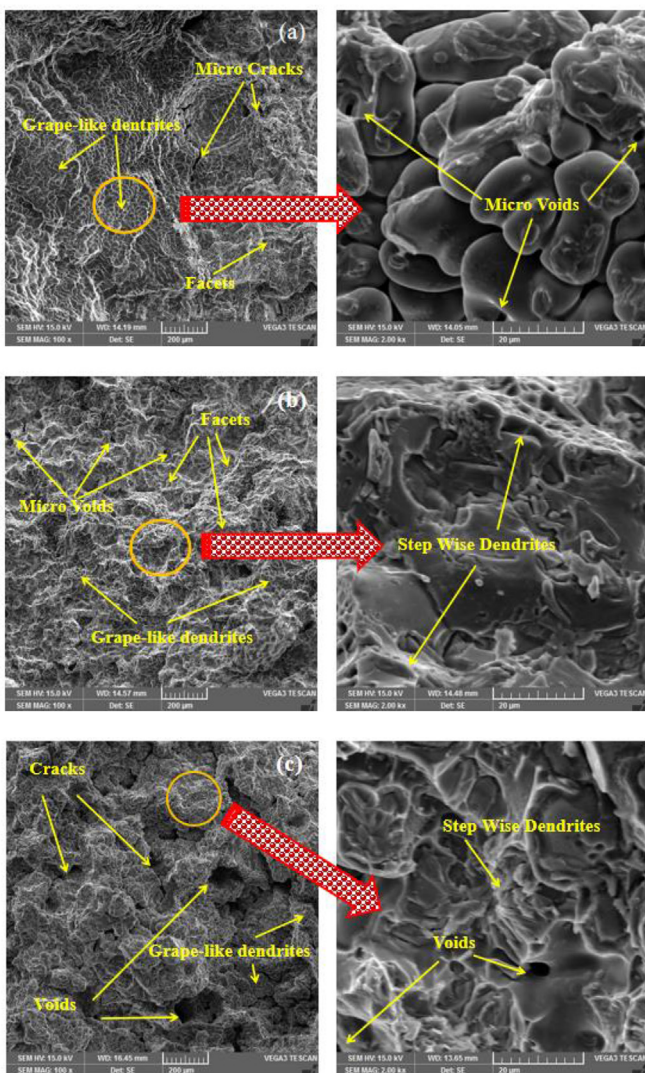

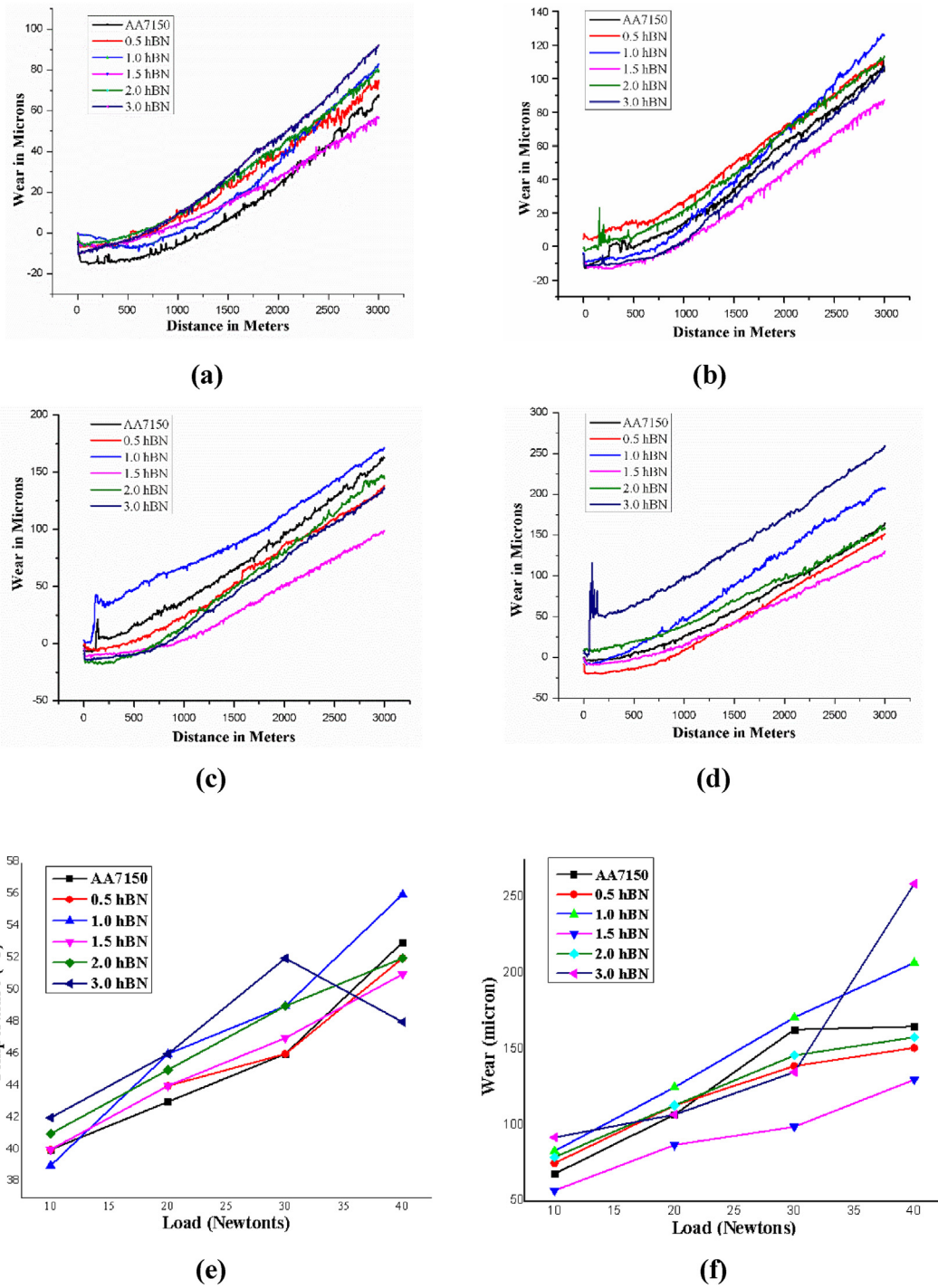**Fig. 7.** SEM images of tensile fracture surface (a) Al7150 (b) Al7150-1.5 wt% hBN (c) Al7150−3.0 wt% hBN.

Fig. 8. (a)–(d) Distance vs wear at each load (e)–(g) Load vs temperature, wear, wear rate (h) Wt% vs wear at each load (i) Distance vs wear at 1.5%hBN (j) Coefficient of friction at 40 N.

(g)

(h)

(i)

(j)

Fig. 8. (*continued*).

of 40 N, and reveals more plastic deformation in films as well as deeper grooves due to high frictional temperature, which softens the pin material at coupled region, resulting in massive plastic deformation and oxide layers. From Fig. 9 a-b, it is evident that lower loads lead to more delamination as well as abrasive wear; at higher loads heavy plastic deformation results.

Fig. 9 c shows the worn surface of 1.5 wt% hBN nanocomposite at a load of 40 N, and indicates the abrasive wear with deeper grooves due to increase in hBN wt.%; therefore, the plastic deformation is restricted and acts as a protective film, which results in minimum surface damage. Fig. 9 d displays the worn surface of 3 wt% hBN nanocomposite at 40 N load, revealing more delamination, debris and oxide layer formation on wear surface.

4. Conclusions

The MMCs of Al7150-hBN nanocomposites were fabricated and the influence of hBN nanoparticles reinforcement was investigated on mechanical, tribological and the following conclusions were inferred. Ultrasonic assisted double stir casting technique and vortex methods were used to fabricate the novel Al7150-hBN nanocomposites with uniformly distributed hBN nanoparticles.

1. XRD and EDS analysis revealed the major elements of Al7150 alloy and hBN nanoparticles presence in the matrix alloy with no impurities.
2. Increase in hBN wt%, increased the hardness and strength (151.3–180.2 H V and 141–255 MPa) of the nanocomposites due to uniform distribution, grain refinement and hard phase particles, which promotes load bearing capacity. Further increment in hBN wt% decreases the hardness and strength (180.2–160.8 H V and 255-216 MPa) due to voids, clusters and agglomerations.
3. Microstructure analysis of Al7150-hBN nanocomposites OM & SEM reveals the grain refinement, nanoparticle distribution and exact nature of failure in nanocomposites.
4. Wear loss of nanocomposites decreased with the increase in the hBN nanoparticles reinforcement due to hardness enhancement, which leads to seizure and wear resistance.
5. Graphical representation of wear results confirmed that the load has greatest influence on wear loss and temperature due to higher frictional forces.
6. SEM images of wear surface reveals that the wear is an abrasive type with restricted plastic deformation and acted as protective layer at 1.5 wt% hBN. 3 wt% hBN reveals more debris, oxide layer and delamination on wear surfaces.
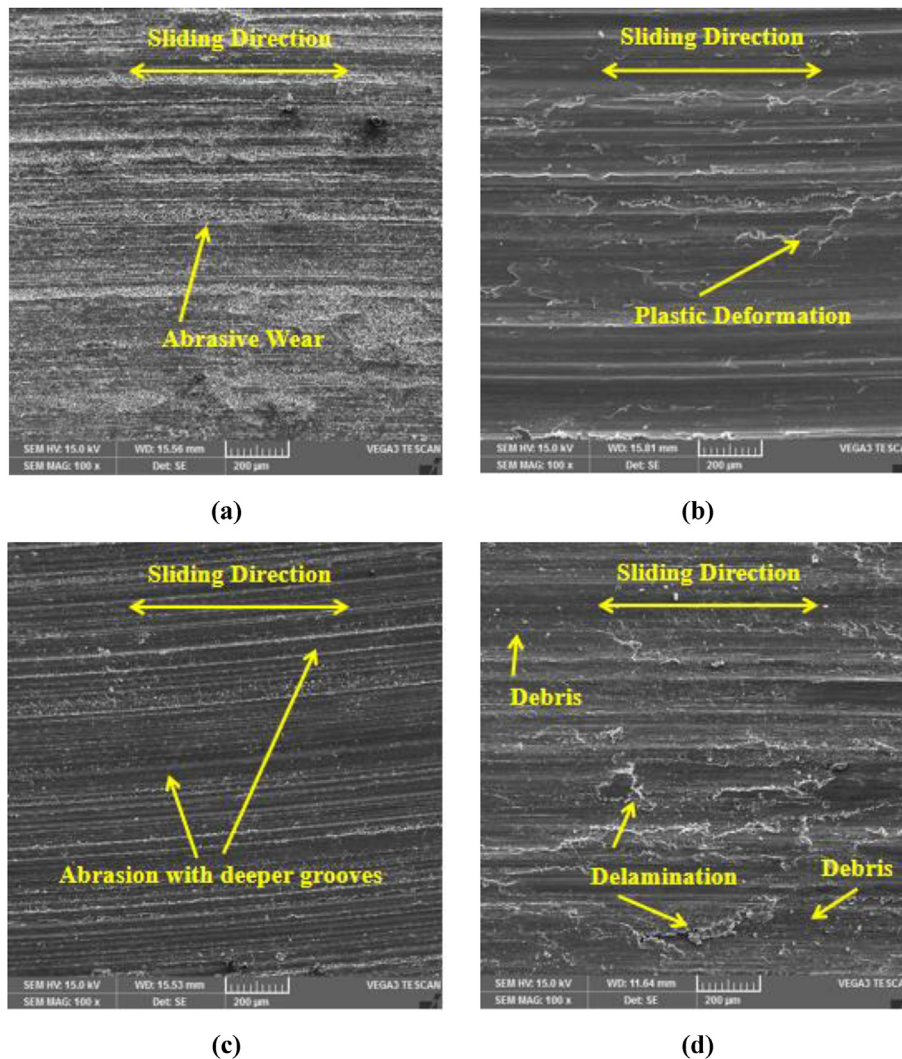
Fig. 9. SEM images of wear surface (a) AA7150 at minimum load (b) AA7150 at maximum load (c) AA7150−1.5%hBN at maximum load (d) AA7150-3%hBN at maximum load.

References

[1] T. Prater, Friction stir welding of metal matrix composites for use in aerospace structures, Acta Astronaut. 93 (2014) 366−373.

[2] D. Mandal, S. Viswanathan, Effect of heat treatment on microstructure and interface of SiC particle reinforced 2124 Al matrix composite, Mater. Char. 85 (2013) 73−81.

[3] Niloofar Soltani, S.K. Sadrnezhaad, Bahrami Amin, Manufacturing wear-resistant 10Ce-TZP/Al2O3 nanoparticle aluminum composite by powder metallurgy processing, Mater. Manuf. Process. 29 (2014) 1237−1244.

[4] Hai Su, Wenli Gao, Hui Zhang, Hongbo Liu, Jian Lu, Zheng Lu, Optimization of stirring parameters through numerical simulation for the preparation of aluminum matrix composite by stir casting process, J. Manuf. Sci. Eng., ASME 132 (2010), 061007.

[5] S.A. Sajjadi, M.T. Parizi, H.R. Ezatpour, A. Sedghi, Fabrication of A356 composite reinforced with micro and nano Al2O3 particles by a developed compocasting method and study of its properties, J. Alloy, Compd 511 (2012) 226−231.

[6] Mingfang Qian, Xuexi Zhang, Jianchao Li, Xiang Gao, Lin Geng, Microstructure and mechanical properties of ABOw and nickel-coated MWCNTs reinforced 2024Al hybrid composite fabricated by squeeze casting, Mater. Chem. Phys. 226 (2019) 344−349.

[7] N. Soltani, HR Jafari Nodooshan, A. Bahrami, M.I. Pech-Canul, Wencai Liu, Gouhua Wu, Effect of hot extrusion on wear properties of Al−15 wt.% Mg2Si in situ metal matrix composites, Mater. Des. 53 (2014) 774−781.

[8] A. Bahrami, M.I. Pech-Canul, C.A. Gutierrez, N. Soltani, Effect of rice-husk ash on properties of laminated and functionally graded Al/SiC composites by one-step pressureless infiltration, J. Alloy. Comp. 644 (2015) 256−266. https://doi.org/10.1016/j.jallcom.2015.04.194.

[9] N. Soltani, S. Soltani, A. Bahrami, M.I. Pech-Canul, L.A. Gonzalez, A. Möller, J. Tapp, A. Gurlo, Electrical and thermomechanical properties of CVI-Si3N4 porous rice husk ash infiltrated by Al-Mg-Si alloys, J. Alloy. Comp. 696 (2017) 856−868.

[10] A. Bahrami, N. Soltani, M.I. Pech-Canul, S. Soltani, L.A. González, C.A. Gutiérrez, J. Tapp, A. Möller, A. Gurlo, Bilayer graded Al/B4C/rice husk ash composite: wettability behavior, thermo-mechanical, and electrical properties, J. Compos. Mater. 52 (2018) 3745−3758.

[11] Jufu Jiang, Ying Wang, Microstructure and mechanical properties of the semisolid slurries and rheoformed component of nano-sized SiC/7075 aluminum matrix composite prepared by ultrasonic- assisted semisolid stirring, Mater. Sci. Eng., A 639 (2015) 350−358.

[12] P. Madhukar, N. Selvaraj, C.S.P. Rao, Manufacturing of aluminium nano hybrid composites: a state of review, IOP Conf. Ser. Mater. Sci. Eng. 149 (2016) 12114.

[13] A. Mazahery, M.O. Shabani, Mechanical properties of A356 matrix composites reinforced with nano-SiC particles, Strength Mater. 44 (2012) 686−692.

[14] Y. Yang, J. Lan, X.C. Li, Study on bulk aluminum matrix nano-composite fabricated by ultrasonic dispersion of nano-sized SiC particles in molten aluminium alloy, Mater. Sci. Eng., A 380 (2004) 378−383.

[15] Y. Yang, X. Li, Ultrasonic cavitation based nanomanufacturing of bulk

aluminum matrix nanocomposites, J. Manuf. Sci. Eng., ASME 129 (2007) 252—255.

[16] Guoping Cao, Hiromi Konishi, Xiaochun Li, Mechanical properties and microstructure of Mg/SiC nanocomposites fabricated by Ultrasonic cavitation based nano-manufacturing, J. Manuf. Sci. Engg., ASME 130 (2008), 031105.

[17] J. Lan, Y. Yang, X. Li, Microstructure and microhardness of SiC nanoparticles reinforced composite fabricated by ultrasonic method, Mater. Sci. Eng., A 386 (2004) 284—290.

[18] Qiang Li, Feng Qiu, Bai—Xin Dong, Run Geng, Ming—ming Lv, Qing—Long Zhao, Qi-Chuan Jiang, Fabrication, microstructure refinement and strengthening mechanisms of nanosized SiCP/Al composites assisted ultrasonic vibration, Mater. Sci. Eng., A 735 (2018) 310—317.

[19] Wei-Si Tian, Qing-Long Zhao, Qing-Quan Zhang, Feng Qiu, Qi-Chuan Jiang, Enhanced strength and ductility at room and elevated temperatures of Al-Cu alloy matrix composite reinforced with bimodal-sized TiCp compared with monomodal—sized TiCp, Mater. Sci. Eng., A 724 (2018) 368—375.

[20] S. Mahathanabodee, T. Palathai, S. Raadnui, R. Tongsri, N. Sombatsompop, Effects of hexagonal boron nitride and sintering temperature on mechanical and tribological properties of SS316L/h-BN composites, Mater. Des. 46 (2013) 588—597.

[21] Gisele Hammes, Kelen Juliane Mucelin, Priscilada Costa Gonçalves, Cristiano Binder, Roberto Binder, Rolf Janssen, Aloisio Nelmo Klein, José Daniel Biasolide Mello, Effect of hexagonal boron nitride and graphite on mechanical and scuffing resistance of self-lubricating iron based composite, Wear 376 (2017) 1084—1090.

[22] X. Liu, C. Zhang, Z. Zhang, J. Xue, Q. Le, The role of ultrasound in hydrogen removal and microstructure refinement by ultrasonic argon degassing process, Ultrason. Sonochem. 38 (2017) 455—462.

[23] G.I. Eskin, D.G. Eskin, Production of natural and synthesized aluminum-based composite materials with the aid of ultrasonic (cavitation) treatment of the melt, Ultrason. Sonochem. (10) (2003) 297—301, 2003.

[24] H. Puga, J. B, E. Seabra, The influence of processing parameters on the ultrasonic degassing of molten AlSi9Cu3 aluminium alloy, Mater. Lett. 63 (2009) 806—808.

[25] Temel Varol, Aykut Canakci, The effect of type and ratio of reinforcement on the synthesis and characterization Cu-based nanocomposites by flake powder metallurgy, J. Alloy. Comp. 649 (2015) 1066—1074.

[26] N. Soltani, M.I. Pech-Canul, A. Bahrami, Effect of 10Ce-TZP/Al2O3 nanocomposite particle amount and sintering temperature on the microstructure and mechanical properties of Al/(10Ce-TZP/Al2O3) nanocomposites, Mater. Des. 50 (2013) 85—91.

[27] Lian-Yi Chen, Jun-Yang Peng, Jia-Quan Xu, Hongseok Choi, Xiao-Chun Li, Achieving uniform distribution and dispersion of a high percentage of nanoparticles in metal matrix nanocomposites by solidification processing, Scr. Mater. 69 (2013) 634—637.

[28] Pagidi Madhukar, N. Selvaraj, C.S.P. Rao, G.B. Veeresh Kumar, Tribological Behavior of Ultrasonic Assisted Double Stir Casted Novel Nano-Composite Material (AA7150-hBN) Using Taguchi Technique, Composites Part B, 2019, p. 107136.

[29] G.B. Veeresh Kumar, C.S.P. Rao, N. Selvaraj, Studies on mechanical and dry sliding wear of Al6061—SiC composites, Composites Part B 43 (2012) 1185—1191.

[30] Pagidi Madhukar, N. Selvaraj, Raghavendra Gujjala, Chilakalapalli Surya Prakasa Rao, Production of high performance AA7150-1% SiC nanocomposite by novel fabrication process of ultrasonication assisted stir casting, Ultrason. Sonochem. 58 (2019) 104665.

[31] K.L. Firestein, S. Corthay, A.E. Steinman, A.T. Matveev, A.M. Kovalskii, I.V. Sukhorukova, D. Golberg, D.V. Shtansky, High-strength aluminum-based composites reinforced with BN, AlB2 and AlN particles fabricated via reactive spark plasma sintering of Al-BN powder mixtures, Mater. Sci. Eng., A 681 (2017) 1—9.

[32] K.L. Firestein, A.E. Steinman, I.S. Golovin, J. Cifre, E.A. Obraztsova, A.T. Matveev, A.M. Kovalskii, O.L. Lebedev, D.V. Shtansky, D. Golberg, Fabrication, characterization, and mechanical properties of spark plasma sintered Al—BN nanoparticle composites, Mater. Sci. Eng. A 642 (2015) 104—112.

[33] Suiyuan Chen, Yuning Bi, Honlon Zhang, Jing Liang, Wellburn Dan, L.I.U. Chang-sheng, Effect of BN fraction on the mechanical and tribological properties of Cu alloy/BN self-lubricating sleeves, J. Compos. Mater. 30 (2015) 3715—3725.

[34] A. Rushikesh, Khatavkar, K. Abhijeet, D. Mandave, Baviskar Devakant, Samir

[35] L. shinde, Influence of hexagonal boron nitride on tribological properties of AA2024-hBN metal matrix composite, I. Res. J. Eng. Tech. 5 (2018) 3792.

[35] R. Deaquino-Lara, N. Soltani, A. Bahrami, E. Gutiérrez-Castañeda, E. García-Sánchez, M.A.L. Hernandez-Rodríguez, Tribological characterization of Al7075—graphite composites fabricated by mechanical alloying and hot extrusion, Mater. Des. 67 (2015) 224—231.

[36] C. Chen, L. Guo, J. Luo, J. Hao, Z. Guo, A.A. Volinsky, Aluminum powder size and microstructure effects on properties of boron nitride reinforced aluminum matrix composites fabricated by semi-solid powder metallurgy, Mater. Sci. Eng. A 646 (2015) 306—314.

[37] Z. Wang, K. Georgarakis, K.S. Nakayama, Y. Li, A.A. Tsarkov, G. Xie, D. Dudina, D.V. Louzguine-Luzgin, A.R. Yavari, Microstructure and mechanical behavior of metallic glass fiber reinforced Al alloy matrix composite, Nature-Scientific Reports 6 (2016) 24384.

[38] Sankaranarayanan Seetharaman, Jayalakshmi Subramanian, Khin Sandar Tun, Abdelmagid Hamouda, Manoj Gupta, Synthesis and characterization of nano boron nitride reinforced Magnesium composites produced by the microwave sintering method, Mater 6 (2013) 1940—1955.

[39] A. Erman, J. Groza, X. Li, H. Choi, G. Cao, Nanoparticle effects in cast Mg-1 wt% SiC nano-composites, Mater. Sci. Eng. A 558 (2012) 39—43.

[40] W.S. Cho, Z.H. Piao, K.J. Lee, Y.C. Yoo, J.H. Lee, M.W. Cho, Y.C. Hong, K. Park, W.S. Hwang, Microstructure and mechanical properties of AlN—hBN based machinable ceramics prepared by pressureless sintering, J. Eur. Ceram. Soc. 27 (2007) 1425—1430.

[41] T. Thirumalai, R. Subramanian, S. Kumaran, S. Dharmalingam, S.S. Ramakrishnan, Production and characterization of hybrid aluminum matrix composites reinforced with boron carbide (B4C) and graphite, J. Sci. Ind. Res. 73 (2014) 667—670.

[42] M.A. Easton, M.A. Qian, D H St John, Grain Refinement in Alloys: Novel Approaches, Encyclopedia of Materials: Science and Technology, second ed., Elsevier, Oxford, 2011, pp. 1—7.

[43] Alireza Moradkhani, Hamidreza Baharvandi, Microstructural analysis of fracture surfaces and determination of mechanical properties of Al2O3—SiC—MgO nanocomposites, Int. J. Refract. Metals Hard Mater. 67 (2017) 40—55.

[44] M.A. Maleque, A.A. Adebisi, N. Izzati, Analysis of fracture mechanism for Al-Mg/SiCp composite materials, Mater. Sci. Eng. 184 (2017), 012031.

[45] A. Pineau, A.A. Benzerga, T. Pardoen, Failure of metals I: brittle and ductile fracture, Acta Mater. 107 (2016) 424—483.

[46] Alaa Mohammed Razzaq, Dayang Laila Majid, Mohamad R. Ishak, Uday M. Basheer, Effect of fly ash addition on the physical and mechanical properties of AA6063 alloy reinforcement, Metal 7 (2017) 477.

[47] A. Baradeswaran, A. Elaya Perumal, Study on mechanical and wear properties of Al 7075/Al2O3/graphite hybrid composites, Composites Part B 56 (2014) 464—471.

[48] N. Selvakumar, S.C. Vettivel, Thermal, electrical and wear behavior of sintered Cu—W nano composite, Mater. Des. 46 (2013) 16—25.

[49] A. Baradeswaran, A. Elaya Perumal, R. Franklin Issac, A Statistical analysis of optimization of wear behaviour of Al-Al2O3 composites using Taguchi technique, Proced. Eng. 64 (2013) 973—982.

[50] G.B. Veeresh Kumar, R. Pramod, P.S. Gouda, C.S.P. Rao, Effect of tungsten carbide reinforcement on the aluminium 6061 alloy, J. Test. Eval. 47 (2018) 1—32.

[51] T.S. Kiran, M. Prasanna Kumar, S. Basavarajappa, B.M. Viswanatha, Dry sliding wear behavior of heat treated hybrid metal matrix composite using Taguchi techniques, Mater. Des. 63 (2014) 294—304.

[52] A. Baradeswaran, S.C. Vettivel, A. Elaya Perumal, N. Selvakumar, R. Franklin Issac, Experimental investigation on mechanical behaviour, modelling and optimization of wear parameters of B4C and graphite reinforced aluminium hybrid composites, Mater. Des. 63 (2014) 620—632.

[53] R. Kumar, S. Dhiman, A study of sliding wear behaviors of Al-7075 alloy and Al- 7075 hybrid composite by response surface methodology analysis, J Mater. Des. 50 (2013) 351—359.

[54] Xiuqing Lia, Yimin Gao, Shizhong Wei, Qingxia Yang, Zhichao Zhong, Dry sliding tribological properties of self-mated couples of B4C-hBN ceramic composites, Ceram. Int. 43 (2017) 162—166.

[55] S. Kovacik, J. Emmer, L. Bielek, L. Kelesi, Effect of composition on friction coefficient of Cu—graphite composites, Wear 265 (2008) 417—421.

[56] Baradeswaran, A. Elayaperumal, Effect of graphite content on tribological behaviour of aluminium alloy—graphite composite, Eur. J. Sci. Res. 53 (2011) 163—170.